EPJ manuscript No.
(will be inserted by the editor)

A Precise Measurement of $sin^2\theta_W$ at Low Q^2 in Møller Scattering

Antonin Vacheret and David Lhuillier, representing the E-158 Collaboration

CEA-Saclay, Dapnia/SPhN, 91191 Gif-sur-Yvette

Received: December 23, 2004/ Revised version: December 23, 2004

Abstract. The E-158 experiment has performed the first measurement of the parity-violating asymmetry in electron-electron (Møller) scattering. Using a 50 GeV polarized electron beam and a fixed unpolarized liquid hydrogen target in End Station A at SLAC. Our preliminary results is: $A_{PV} = -128 \pm 14(stat) \pm 12(syst) \times 10^{-9}$. From this quantity we extract $\sin^2\theta_W(Q^2 = 0.026 GeV/c^2)_{\overline{MS}} = 0.2403 \pm 0.0010(stat) \pm 0.0009(syst)$, consistent with the Standard Model prediction.

PACS. 11.30.Er Charge conjugation, parity, time reversal, and other discrete symmetries – 12.15.Lk Electroweak radiative corrections – 12.15.Mm Neutral currents – 13.66.Lm Processes in other lepton-lepton interactions – 13.88.+e Polarization in interactions and scattering – 14.60.Cd Electrons

1 Introduction and physics motivation

In the scattering of longitudinally polarized electrons from unpolarized targets, the reversal of the helicity of incoming electrons is equivalent to applying the parity symmetry. Hence the quantity $A_{PV} = (\sigma_R - \sigma_L)(\sigma_R + \sigma_L)$, where $\sigma_{R,L}$ is the cross section for incident right(left)-handed electrons, is a pseudo-scalar arising from the parity violating part of the interaction in the scattering process. To first order this corresponds to the interference of the neutral weak and electromagnetic amplitudes[1]. When considering the Møller process, A_{PV} is proportional to the electron's weak charge, written at tree level as $Q_W^e = 1 - 4\sin^2\theta_W$ where θ_W is the weak mixing angle. The motivation of the E158 experiment is to measure $\sin^2\theta_W$ at low energy[2], far away from the Z-pole ($Q^2 \ll M_Z^2$) where precise measurements of this parameter have already been performed by the SLD and LEP collaborations[3]. The high accuracy we are seeking ($< 1\%$ relative error on $\sin^2\theta_W$) requires to include radiative corrections in the expression of A_{PV}:

$$A_{PV} = \frac{G_F Q^2}{\sqrt{2}\pi\alpha} \frac{1-y}{1+y^4+(1-y)} \mathcal{F}_b \, Q_W^e(Q^2) \qquad (1)$$

where G_F and α are the Fermi and fine structure constants, Q^2 is the square of the four-vector momentum transfer and $y = Q^2/s$, where s is the square of the center-of-mass energy. The $\mathcal{F}$ factor accounts for photon radiation effects in initial and final states. Most of the loop and vertex electroweak corrections are absorbed into the definition of an effective weak mixing angle $\sin^2\theta_W(Q^2)$ which acquires a Q^2 dependence. Taking advantage of the large cross section and little theoretical uncertainty of the purely leptonic Møller reaction, a precise measurement of these electroweak radiative corrections probes physics beyond the Standard Model (SM) at the TeV scale.

The figure of merit of the measurement peaks at high energy and to less extent at center-of-mass scattering angles around 90°. With a 50 GeV beam and $Q^2 = 0.026\,\mathrm{GeV/c^2}$, A_{PV} is predicted to be $\simeq$320 parts per billion (ppb) at tree level. Electroweak radiative corrections[4] reduce $\sin^2\theta_W$ by 3%. However this quantity remains numerically very close to 1/4 resulting in an experimental asymmetry reduced by more than 40%. Hence the difficulty of measuring an extremely small asymmetry is compensated by a great sensitivity to $\sin^2\theta_W$.

2 Beam

The development of the intense and highly polarized 50 GeV beam in SLAC End Station A (ESA) is a key element in the measurement of A_{PV}. Longitudinally polarized electrons are produced by optical pumping of a strained GaAs photo-cathode[5] by circularly polarized laser light. The sign of the laser circular polarization state determines the electron beam helicity. The beam is pulsed at 120 Hz with an intensity of 5.10^{11} electrons in a 300 ns pulse. The time structure consists of quadruplets of two consecutive pulses with pseudo-randomly chosen helicities, followed by their complements, yielding two independent left-right pulse pairs every 33 ms. This sequence is phase-locked to the 60 Hz of the power line in order to reduce electronic noise. One of the main experimental challenges when measuring a physics asymmetry at the few 100 ppb level is to keep the beam parameters (intensity, energy, position, angle) with negligible left-right asymmetries. The strategy used to reduce these asymmetries is three-fold[6]: a passive minimization of helicity correlated intensity and position differences that result from imperfections in the laser light and the photo-cathode response is first performed by a

careful optimization of all the optical elements in the laser path. Then helicity-dependent corrections are applied to the laser beam in a feedback loop using periodic average measurement of beam asymmetries at upstream and downstream ends of the accelerator. This measurements are performed by cavity monitors implemented by pairs on the beam line [8]. This redundancy is critical to access the intrinsic resolution of the monitors and be able to read the beam parameters with a precision far better than their pulse to pulse jitter. Finally a set of slow reversals, performed on a 1 or 2 days basis, further suppress effects of the remaining asymmetries. A half-wave plate can be inserted across the laser beam of the source to flip its polarization. Also the main linac can be operated at 45.6 or 48.7 GeV resulting in a 180° extra spin precession in the arc leading to ESA. In both cases the electron beam helicity is flipped, hence the sign of A_{PV}, while certain classes of beam asymmetries remain unaffected yielding to partial cancellations. Thanks to these active minimizations, cumulative beam asymmetries are reduced to < 200 ppb in intensity, < 10 ppb in energy, and < 5 nm in position, orders of magnitude below the "natural" beam asymmetries one could expect from the accelerator.

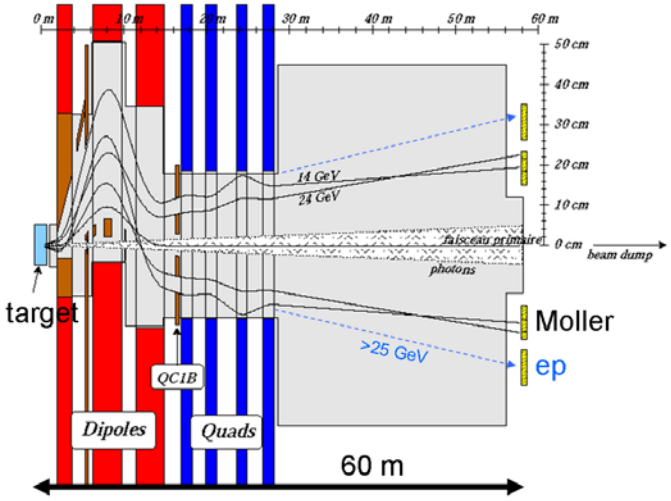

Fig. 1. Overview of the experimental setup in ESA. The horizontal axis is shrunk by a factor ≃50 in order to enhance the horizontal deviation of the dipole chicane and the focusing of the Møller events toward the inner crown of detectors.

3 Instrumentation in ESA

The apparatus in ESA is illustrated in Fig.1. The high luminosity and good background rejection required for the measurement of the tiny Møller asymmetry are achieved by the use of an extended target, a spectrometer/collimator system and integrating detectors.

The target cell [7] is a 1.57 m long cylinder filled with liquid hydrogen circulating at ≃5 m/s. Turbulences are enhanced by Aluminum meshes in the fluid path allowing the absorption of ≃500 W deposited by the beam while keeping density fluctuations below 40 ppm per pulse pair. These fluctuations are monitored by "luminosity monitors" consisting of eight ionization chambers arranged around the beam pipe downstream the detectors and intercepting particles scattered at ≃1 mr. The huge rate provides great sensitivity to target boiling as well as a powerful check of the null asymmetry expected at such forward angles. The choice of hydrogen as an electron target results from the best Z/A ratio.

The low Q^2 and high energy kinematics lead to very forward laboratory scattering angles and both the primary beam and the scattered particles propagate through the spectrometer. A horizontal 3-dipole chicane defines the energy acceptance and shields the detectors from direct line-of-sight to the target. At the exit of the chicane the primary beam is put back on its axis and the main acceptance collimator, 3QC1B, selects particles between 4.4 and 7.5 mr. Then a series of 4 quadrupoles separates spatially the Møller-scattered electrons from the Mott (*ep* scattering) background at the detector plane 60 meters downstream the target. Selected Møller electrons form a ring approximately symmetric about the beam axis with an energy range of 13-24 GeV and containing ≃2.10^7 electrons per pulse. For the asymmetry measurement, the particles are intercepted by the Møller and *ep* detectors, consisting of 25 cm thick concentric cylinders with a 15-25 cm and 25-35 cm radius coverage respectively. They are assembled by layering planes of flexible fused-silica fibers between elliptical copper plates so as to withstand a 100 Mrad radiation dose. The fibers are oriented at the Cherenkov angle and gathered in bunches at the back of the detector. They direct the Cherenkov light into shielded PMTs via air light-guides. A total of 60 bunches provides radial and azimuthal segmentation (Fig.2). The asymmetry is simply measured by extracting the fractional difference in the integrated calorimeter response for incident right- and left-handed beam pulses. This technique allows reaching very high counting rate with no dead time. The drawback is a "blind" detector integrating all events in the acceptance, including background. Therefore a complete set of auxiliary detectors is implemented to monitor the flux and the asymmetry of the different backgrounds.

A profile detector is located just upstream of the main calorimeter providing a complete radial and azimuthal map of the charged particles flux. Numerous profile measurements allow a very accurate calibration of the simulations (Fig.2). The dominant background is the *ep* flux with 8% contamination of the Møller flux. The small contribution of photons and neutrons to the calorimeter response is measured in calibration runs. The pion flux and asymmetry are measured behind the Møller detector and a heavy lead shielding using a set of 10 Cherenkov detectors.

Finally the beam polarization is measured once every 2 days using a polarized supermendur foil target just upstream the LH2 target. Thanks to a dedicated retractable collimator, doubly-polarized Møller events are isolated inside a small element of the acceptance of the same spectrometer as for the main experiment. They are detected by a small tungsten/quartz stack fixed at the end of an

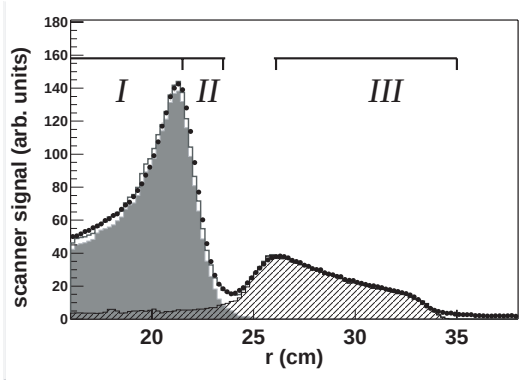

Fig. 2. Radial profile of charged particles at the calorimeter. The points are data, the histograms are simulations of the Møller (shaded) and *ep* (hatched) flux. For the detection of Møller electrons, regions I+II are segmented in three rings of 10, 20 and 20 PMTs respectively.

air light-guide with PMT readout. This setup is mounted on the profile detector frame.

4 Analysis and Preliminary Results

Every 33 ms the data from all beam monitors and detector channels are collected for the 4 beam pulses of a quadruplet. The experimental detector asymmetries (A_{exp}) and beam parameters differences (Δx_i, $i = E, x, y, \theta_x, \theta_y, Q$) for the corresponding two pairs are extracted. The analysis is performed with a blinding offset added to the detector asymmetries. This offset is picked-up by a random algorithm in a range comparable to the expected physics asymmetry and kept secret until the very last stage of the analysis, preventing any psychological influence on the final results. The cuts applied to the data (16% of rejected events) select periods of stable beam and operational equipement in an helicity-independent way. In total $\approx 4 \times 10^8$ pulse pairs satisfy all criteria for the three runs taken in 2002-3. Final results have already been published for the first run[9], we present here preliminary results for the complete statistics.

The detector signals are corrected for differences in the right-left beam properties as measured by the beam monitors according to

$$A_{raw} = A_{exp} - \sum_i \alpha_i \Delta x_i \qquad (2)$$

where the coefficients α_i are the sensitivities of the detector to each beam parameter. They are determined by two independent methods. The first one applies an unbinned least squares linear regression to the pulses used for physics, taking advantage of the beam parameters jitter. The second method, so-called "dithering", uses calibration subset of the pulses (4% duty cycle), where each parameter is modulated periodically around its average value by an amount large compared to beam jitter. Because of its very forward kinematics E-158 is quite sensitive to beam fluctuations therefore the extra lever arm given by the large amplitudes of the dithering method is not critical to extract accurate α coefficients. Final analysis relies on the first method, statistically more powerfull, and uses the dithering as a cross-check of systematic errors. These corrections remove both the beam-induced random and systematic effects. The RMS of the A_{raw} distribution is reduced to ≈200 ppm, very close to the expected pure statistical width and a factor 2 smaller than the RMS of the A_{exp} distribution. The cumulative asymmetry correction is listed in table 1 for run III. The impressively small systematic error of 1 ppb follows from the excellent agreement between the two correction methods when applied on the same data sample.

Table 1. Corrections ΔA and dilutions f to A_{raw} for run III.

Source	ΔA (ppb)	f
Beam (first order)	1 ± 1	-
Beam (higher order)	0 ± 4	-
Transverse polarization	-4 ± 2	-
$e^- p \to e^- p(+\gamma)$	-8 ± 2	0.058 ± 0.007
$e^-(\gamma) p \to e^- p(+\gamma)$	-22 ± 6	0.009 ± 0.003
High energy photons	3 ± 3	0.004 ± 0.002
Synchrotron photons	0 ± 2	0.0015 ± 0.0005
Neutrons	-1 ± 1	0.0006 ± 0.0002
Pions	1 ± 1	0.001 ± 0.001

After correcting the effects of all the beam parameters non-statistical fluctuations of A_{raw} around its mean value are observed in the, most sensitive, outer crown of the Møller detector, pointing to extra systematic effects at the sub-pulse scale. Such effects couldn't be treated with the above-mentioned methods which only deal with mean values per pulse. To study and correct the induced false asymmetries the signals of the beam monitors are oversampled with 4 time-slices inside the duration of a beam pulse. The final correction removes all the non-statistical fluctuations with no significant effect on the mean value and a total systematic error of 4 ppb.

After a complete regression a remaining azimuthal modulation of A_{raw} is observed due to a small non-zero component of the transverse beam polarization leading to a correction of -4 ± 2 ppb. A separate study limited the bias due to beam spot-size fluctuations on A_{raw} to 1 ppb, using data from a retractable wire array.

The physics asymmetry is finally formed from A_{raw} by correcting for background contributions, detector linearity ϵ and beam polarization P_e:

$$A_{phys} = \frac{1}{P_e \epsilon} \frac{A_{raw} - \sum_i \Delta A_i}{1 - \sum_i f_i} \qquad (3)$$

where ΔA_i and f_i are the asymmetry corrections and dilutions for various background sources listed in table 1. The largest correction is due to electrons from inelastic electron- and photon-proton interactions. The associated asymmetry was measured during the first run in the *ep* detector and reasonable assumptions were used for the kinematic extrapolation to the Møller region. The flux

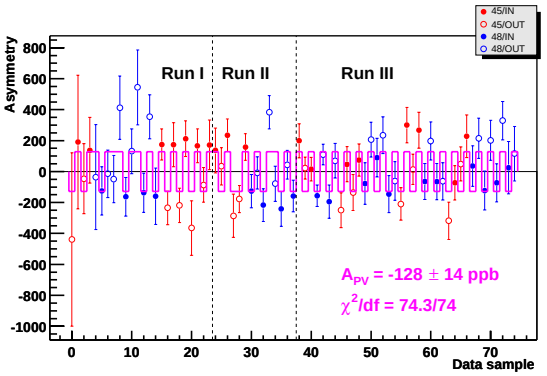

Fig. 3. Møller physics asymmetry. The solid line indicates the expectation for the asymmetry for all combinations of beam energy and half-wave plate state.

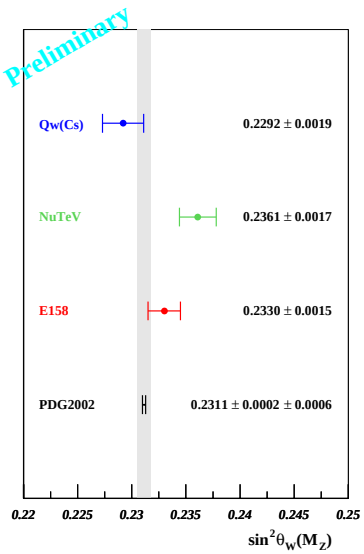

Fig. 4. Summary of $\sin^2\theta_W(\overline{MS})$ measurements evolved to the Z-pole. $Q_W(Cs)$: parity violation in Cesium atoms, NuTeV: ν-nuclei scattering, PDG2002: world average, see [14].

contamination is determined from a simulation validated with the numerous profile detector data.
The averaged beam polarization is $88 \pm 5\%$ with dominant errors arising from the knowledge of the magnetization of the foil target and the background. The linearity of the calorimeter response is determined to be $\epsilon = 0.99 \pm 0.01$.
As a final check the mean A_{phys} is plotted for each of the energy and half-wave plate configurations. Figure 3 show that data are compatible with a perfect sign reversal, giving confidence in the removal of all spurious asymmetries. After removing the blinding offset the grand average of the sign corrected asymmetries gives to the final physics result:

$$A_{PV} = -128 \pm 14\,(stat.) \pm 12\,(syst.)\ \text{ppb} \qquad (4)$$

establishing parity violation in Møller scattering at the 8 σ level, the most precise measurement of any asymmetry in electron scattering. Using Eq.(1) we can extract the weak charge of the electron and then $\sin^2\theta_W(Q^2)$. The average kinematics as well as photon radiation effect are determined from a Monte Carlo simulation: $Q^2 = 0.026\ (\text{GeV/c})^2$, $y \simeq 0.6$ and $\mathcal{F}_b = 1.01 \pm 0.01$. We find

$$\sin^2\theta_W(Q^2 = 0.026\,\text{GeV/c}^2)_{\overline{MS}} = \qquad (5)$$
$$0.2403 \pm 0.0010\,(stat) \pm 0.0009\,(syst)$$

consistent at the 1.2 σ level with the SM expectation [4] $\sin^2\theta_W(0)_{\overline{MS}} = 0.2385 \pm 0.0006\,(theory)$. This result provides significant new limits on physics beyond the SM. For example the scale Λ_{LL} of a new left-handed contact interaction [10] is set to $\Lambda^+_{LL} \geq 6.4$ TeV and $\Lambda^-_{LL} \geq 13.9$ TeV for potential positive and negative deviations respectively, and the lower limit for the mass of a new Z_χ boson [4] is set to $M_{Z_\chi} \geq 860$ TeV at 95% C.L.
For a coherent comparison between all precise measurements of $\sin^2\theta_W$ figure 4 shows all results evolved to the Z-pole. At low energy the E-158 accuracy is comparable to measurements in the Cesium atoms [11,12] and in ν-nucleon scattering [13]. The significant deviation of the NuTeV result can't be attributed to new physics yet as detailed analysis of nuclear effects is still going on. The sensitivity of the new E-158 result to new physics is complementary to the existing data and the measurement of an asymmetry with a 15 ppb error is a benchmark for future high accuracy experiments [15].

References

1. Ya.B. Zel'dovich, Sov. Phys. JETP **9**4, (1959) 262.
2. K.S. Kumar, R.S. Holmes, E.W. Hughes, and P.A. Souder, Mod. Phys. Lett. **A**10 (1995) 2979.
3. LEP and SLD collaborations, hep-ex/0312023 (2003).
4. A. Czarnecki and W.J. Marciano, Int. J. Mod. Phys. **A**15, (2000) 2365; J. Erler, A. Kurylov, and M.J. Ramsey-Musolf, Phys. Rev. **D**68, (2003) 016006; F.J. Petriello, Phys. Rev. **D**68, (2003) 033006; A. Ferroglia, G. Ossola, and A. Sirlin, eprint hep-ph/0307200 (2003).
5. T. Maruyama *et al.*, Nucl. Inst. Meth. **A**492, (2002) 199.
6. T.B. Humenski *et al.*, Nucl. Inst. Meth. **A**521, (2004) 261.
7. J. Gao *et al.*, Nucl. Instrum. Meth. **A**498, (2003) 90.
8. H. Whittum and Yu. Kolomensky, Rev. Sci. Instrum. **70**, (1999) 2300-2313.
9. P.L. Anthony *et al.*, Phys. Rev. Lett. **9**2, (2004) 181602.
10. M.J. Ramsey-Musolf, Phys. Rev. **C**60, (1999) 015501.
11. C.S.Wood *et al.*, Science **2**75, (1997) 1759
12. V.A. Dzuba, V.V. Flambaum and J.S.M. Ginges, Phys. ReV. **D**66, (2002) 076013; A. Derevianko, B. Ravaine and W.R. Johnson, physics/0401043, (2004).
13. K.S. McFarland, these proceedings and references therein.
14. *Review of Particle Properties*, K. Hagiwara *et al.*, Phys. Rev. **D**66, (2002) 010001.
15. M.J. Ramsey-Musolf, these proceedings and references therein.